

Langevin model for reactive transport in porous media

Alexandre M. Tartakovsky*

Pacific Northwest National Laboratory, Richland, Washington 99352, USA

(Received 24 January 2010; published 5 August 2010)

Existing continuum models for reactive transport in porous media tend to overestimate the extent of solute mixing and mixing-controlled reactions because the continuum models treat both the mechanical and diffusive mixings as an effective Fickian process. Recently, we have proposed a phenomenological Langevin model for flow and transport in porous media [A. M. Tartakovsky, D. M. Tartakovsky, and P. Meakin, *Phys. Rev. Lett.* **101**, 044502 (2008)]. In the Langevin model, the fluid flow in a porous continuum is governed by a combination of a Langevin equation and a continuity equation. Pore-scale velocity fluctuations, the source of mechanical dispersion, are represented by the white noise. The advective velocity (the solution of the Langevin flow equation) causes the mechanical dispersion of a solute. Molecular diffusion and sub-pore-scale Taylor-type dispersion are modeled by an effective stochastic advection-diffusion equation. Here, we propose a method for parameterization of the model for a synthetic porous medium, and we use the model to simulate multicomponent reactive transport in the porous medium. The detailed comparison of the results of the Langevin model with pore-scale and continuum (Darcy) simulations shows that: (1) for a wide range of Peclet numbers the Langevin model predicts the mass of reaction product more accurately than the Darcy model; (2) for small Peclet numbers predictions of both the Langevin and the Darcy models agree well with a prediction of the pore-scale model; and (3) the accuracy of the Langevin and Darcy model deteriorates with the increasing Peclet number but the accuracy of the Langevin model decreases more slowly than the accuracy of the Darcy model. These results show that the separate treatment of advective and diffusive mixing in the stochastic transport model is more accurate than the classical advection-dispersion theory, which uses a single effective diffusion coefficient (the dispersion coefficient) to describe both types of mixing.

DOI: [10.1103/PhysRevE.82.026302](https://doi.org/10.1103/PhysRevE.82.026302)

PACS number(s): 47.56.+r, 05.10.Gg

I. INTRODUCTION

Flow and transport in porous media can be described on the discrete pore (microscopic) scale and the continuum (Darcy) scale, a scale with a characteristic length much larger than the size of a single pore. On the microscopic scale these phenomena are governed by fundamental conservation equations including the continuity equation,

$$\frac{d\rho}{dt} = -\rho \nabla \cdot \mathbf{v}, \quad (1)$$

the momentum conservation (Navier-Stokes) equation,

$$\frac{d\mathbf{v}}{dt} = -\frac{\nabla p}{\rho} + \mathbf{g} + \frac{\mu}{\rho} \nabla \cdot (\nabla \mathbf{v} + \nabla \mathbf{v}^T), \quad (2)$$

and the advection-diffusion equation,

$$\frac{dC}{dt} = \frac{1}{\rho} \nabla \cdot (\rho D_m \nabla C), \quad (3)$$

where \mathbf{v} is the pore-scale fluid velocity, $d/dt = \partial/\partial t + \mathbf{v} \cdot \nabla$, \mathbf{g} is the body force per unit mass and ρ and μ are the density and viscosity of the fluid. C is the solute concentration (mass fraction) and D_m is the molecular diffusion coefficient. On the continuum scale the flow and transport are usually described by Darcy transport equations [2,3] that represent the volumetric or statistical averages of the conservation Eqs.

(1)–(3). These equations consist of the Darcy-scale continuity equation,

$$\frac{d\rho}{dt} = -\rho \nabla \cdot \mathbf{u}, \quad (4)$$

The Darcy flow equation,

$$\frac{d\mathbf{u}}{dt} = -\frac{\nabla p}{\rho} + \mathbf{g} - \gamma \mathbf{u}, \quad (5)$$

and the advection-dispersion equation,

$$\frac{dC}{dt} = \frac{1}{\rho} \nabla \cdot (\rho \mathbf{D} \cdot \nabla C), \quad (6)$$

where \mathbf{u} is the spatially averaged pore-scale fluid velocity and $d/dt = \partial/\partial t + \mathbf{u} \cdot \nabla$. The friction coefficient $\gamma = \phi \mu / (\rho k)$, porosity ϕ , permeability k , and hydraulic conductivity $\phi g / \gamma$, are some of the macroscopic parameters characterizing the continuum properties of porous media. In Eq. (6), C is the solute concentration (defined here as the mass fraction), and \mathbf{D} is the second-rank dispersion tensor.

Due to the complexity of a pore geometry, which results in even greater complexity of pore-scale flow and advection-diffusion processes, and due to the fact that, in general, pore geometry is unknown, it is best to discuss the micro-scale flow in terms of probability density functions of pore-scale velocities and positions of Lagrangian fluid volumes. Usually these probability density functions are non-Gaussian and require an infinite number of moments to be fully described. The Darcy Eqs. (4) and (5) describe fluid mass conservation and the first moment (the average pore velocity) of the pore-

*alexandre.tartakovsky@pnl.gov

scale velocity distribution. The Darcy advection-dispersion Eq. (6) describes the first three moments of the microscale advection-diffusion processes (the zero moment describing the changes of a solute mass; the first moment describing the dynamic of the center of mass, and the second moment describing the variance of a solute plume).

In a homogeneous porous medium, dispersive mixing is the result of a combination of molecular diffusion (diffusive mixing) and spreading due to variations in the pore-scale fluid velocity. The velocity variations inside individual pores, in combination with molecular diffusion, lead to the Taylor-Aris type dispersive mixing. Variations in the direction and magnitude of mean pore velocities in different flow paths due to differences in pore sizes and differences in tortuosities of individual flow paths lead to a larger-scale mechanical mixing between the flow paths. The Darcy-scale flow Eq. (5) describes only averaged fluid velocity. The effect of pore-scale velocity variations on solute spreading leading to the mechanical dispersion is captured by the dispersion tensor in the advection-dispersion equation. The advection-dispersion equation treats the dispersion in homogenous porous media as a Fickian diffusion. Various forms of the dispersion tensor were proposed to describe these types of mixing. For example [4], derived the expressions for dispersion tensor using perturbation analysis, with the longitudinal component of the dispersion tensor having the form:

$$D_L = D_m + \frac{1}{6} \pi^2 \phi \ln(Pe) D_m + \frac{3}{4} Pe D_m, \quad (7)$$

where $Pe = |\mathbf{u}|d/D_m$ is the Peclet number, $|\mathbf{u}|$ is the magnitude of the vector \mathbf{u} , and d is the average soil-grain diameter. In the expression Eq. (7) the first term on the right-hand side describes purely molecular mixing, the second term describes the Taylor-type mixing and the third term, independent of molecular diffusion coefficient, describes purely mechanical mixing. Based on numerous experimental studies, an empirical relationship for the transverse component of the dispersion coefficient was suggested [5,6]:

$$D_T = D_m + aPe^b D_m, \quad (8)$$

where $a < 1$ and $b < 1$ are constants that vary in different studies.

It is common to separate the mechanical mixing from diffusive mixing and Taylor dispersive mixing and use the simpler relationship [2]:

$$D_l = (D_{eff} + \alpha_l |\mathbf{u}|), \quad (9)$$

where α_l ($l=L, T$) are the principal longitudinal (denoted by the subscript L) and transverse (denoted by the subscript T) components of the dispersivity tensor $\boldsymbol{\alpha}$, and D_{eff} is the effective diffusion coefficient. Comparison of Eq. (9) with Eqs. (7) and (8) reveals that the effective diffusion coefficient of porous media is a tensor that depends on D_m and Pe . For moderate and large Pe , the principal components of the effective diffusion tensor are much smaller than $\alpha_T |\mathbf{u}| < \alpha_L |\mathbf{u}|$, and D_{eff} is commonly treated as a scalar constant that depends only on D_m , the porosity and tortuosity of a porous medium [2].

Multicomponent reactive transport with mixing-controlled reactions is one example where the Darcy description can be inadequate. Specifically, the Darcy flow and advection-dispersion equations over predict the extent of mixing controlled reactions [7–9]. Reference [9] found that the error in the Darcy-scale model increases with increasing Pe and is strongly correlated with a dilution index [10] (the dilution index decreases with increasing Pe). Reference [10] demonstrated that a Darcy-scale transport model with constant coefficients overestimates the dilution index and this may lead to over predicting the extent of the mixing controlled reactions.

Recently, we have proposed a phenomenological Langevin model for flow and transport in porous media [1]. The model is based on a Langevin equation that is obtained by adding a white noise into the Darcy flow Eq. (5). In combination with a continuity equation, the Langevin flow equation describes both the first and the second moments of the pore-scale velocity distribution. The velocity obtained from the Langevin flow equation not only advects the center of mass, but also mechanically disperses the solute. Having the velocity field resolved up to the second moment eliminates the need to use the dispersivity tensor $\boldsymbol{\alpha}$ in the Langevin transport model. The diffusion-facilitated dispersion in the Langevin model is governed by a stochastic (due to presence of random advective velocity) advection-diffusion equation. The separate treatment of the mechanical and diffusive mixing produces the mixing zone that is more realistic (in terms of solute dilution) than the mixing zone obtained from the Darcy transport equations.

Random walk models, based on the Ito stochastic differential equation [11], are commonly used to model diffusion and dispersion processes on both the pore and Darcy scales (e.g., [12–16]). The Langevin model and random walk models differ significantly since the random velocity of the fluid in the Langevin model satisfies the continuity equation, while the velocities of the random walkers (tracer particles) do not. The advantages of the Langevin model are: (1) Both molecular diffusion and chemical kinetics can be easily included via the stochastic advection-diffusion equation with appropriate source terms; and (2) Coupling between the flow and changes in the solute concentration field(s) occurs naturally in the model [1,17]. Random walk models belong to the class of discrete models and, in the case of random walk reactive particle models, a result can depend on numerical resolution, e.g., a number of particles ([18] showed that a random walk reactive transport model may not converge with an increasing number of random walkers). The proposed Langevin model is formulated in terms of partial differential equations and the convergence of its solution was demonstrated numerically in [1].

Here, we extend the Langevin model, originally formulated for isotropic dispersion, to the anisotropic dispersion by using an anisotropic white noise in the Langevin equation. We propose a method for parametrization of the Langevin model and we use the model to simulate multicomponent reactive transport in a synthetic two-dimensional porous medium. The detailed comparison of the results of the Langevin model with the pore-scale and the Darcy simulations shows that: (1) for a wide range of Peclet numbers the Langevin

model predicts the mass of reaction product more accurately than the Darcy model; (2) for small Peclet numbers the predictions of both the Langevin and the Darcy models agree well with a prediction of the pore-scale model; and (3) the accuracy of the Langevin model deteriorates with the increasing Peclet number but more slowly than the accuracy of the Darcy model. To provide an accurate comparison, both the Langevin and the Darcy models are parameterized using pore-scale simulations of the advection of a conservative tracer. The transport equations were numerically solved using smoothed particles hydrodynamics (SPH), a Lagrangian particle method that has been previously applied to both deterministic [17,19] and stochastic [20] transport problems.

II. LANGEVIN FLOW AND TRANSPORT MODEL

The Langevin flow and transport model is based on the phenomenological Langevin approach of van Kampen [11]. According to this approach, a macroscale process (such as the mechanical dispersion) driven by the microscale fluctuations (such as pore scale velocity fluctuations) can be modeled by adding white noise (an uncorrelated zero-mean random variable) into the macroscale deterministic equations. The Langevin model is constructed by adding a random force (per unit mass) into the Darcy-scale momentum conservation Eq. (5), and this results in a Langevin equation of the form:

$$\frac{d\mathbf{U}}{dt} = -\frac{\nabla P}{\rho} + \mathbf{g} - \gamma\mathbf{U} + \sqrt{|\langle\mathbf{U}\rangle|}\xi, \quad (10)$$

where $\mathbf{U}(\mathbf{x}, t) = \langle\mathbf{U}(\mathbf{x}, t)\rangle + \tilde{\mathbf{U}}(\mathbf{x}, t)$ and $P(\mathbf{x}, t) = \langle P(\mathbf{x}, t)\rangle + \tilde{P}(\mathbf{x}, t)$ are the random velocity and pressure. Here “ $|\cdot|$ ” denotes a magnitude of a vector, $\langle\cdot\rangle$ denotes the ensemble mean of the random variables, and “ $\tilde{\cdot}$ ” denotes its random deviates.

The random vector variable, $\xi(\mathbf{x}, t) = [\xi_1(\mathbf{x}, t), \xi_2(\mathbf{x}, t), \xi_3(\mathbf{x}, t)]^T$, has a zero ensemble mean, $\langle\xi_i(t)\rangle = 0$, and the covariance function:

$$\langle\xi_i(\mathbf{x}, t)\xi_j(\mathbf{x}', t')\rangle = \Gamma_l^2 \delta(\mathbf{x} - \mathbf{x}') \delta(t - t'), \quad (11)$$

where Γ_l is a constant and δ is the Dirac delta function. The random velocity satisfies the continuity equation:

$$\frac{d\rho}{dt} = -\rho \nabla \cdot \mathbf{U}. \quad (12)$$

Solute transport is described by the classical advection-diffusion equation:

$$\frac{dC}{dt} = \frac{1}{\rho} \nabla \cdot (\rho D_{eff} \nabla C), \quad (13)$$

where C is the solute concentration (defined here as the mass fraction) and $d/dt = \partial/\partial t + \mathbf{U} \cdot \nabla$. Here, D_{eff} is an effective diffusion coefficient representing molecular diffusion and pore-scale Taylor dispersion that depends on D_m and Pe .

The values of $\Gamma_l (l=1, 2, 3)$ can be found by relating the variance of lagrangian displacements $\tilde{\mathbf{X}}$ to a coefficient of mechanical dispersion via Einstein relationship [11]. The la-

grangian displacements in the Langevin model are defined as

$$\mathbf{X}(t) = \langle\mathbf{X}(t)\rangle + \tilde{\mathbf{X}}(t), \quad (14)$$

and

$$\frac{d\mathbf{X}(t)}{dt} = \mathbf{U}(\mathbf{X}^0, t), \quad \mathbf{X}(0) = \mathbf{X}^0. \quad (15)$$

If the direction of averaged velocity $\langle\mathbf{U}\rangle$ coincides with direction 1, then the Einstein relationship takes the form [11]:

$$\lim_{t \rightarrow \infty} \frac{d\langle\tilde{X}_1(t)\tilde{X}_1(t)\rangle}{dt} = 2D_L^M, \quad (16)$$

$$\lim_{t \rightarrow \infty} \frac{d\langle\tilde{X}_l(t)\tilde{X}_l(t)\rangle}{dt} = 2D_T^M, \quad l=2, 3, \quad (17)$$

where D_L^M and D_T^M are the principal components of the mechanical dispersion tensor. Here we define the mechanical dispersion as a dispersion of fluid particles or dispersion of an imaginary tracer with zero diffusion coefficient. If Eq. (9) for the dispersion tensor is assumed, then Γ_l can be related to the dispersivity tensor via the variance of lagrangian displacements as:

$$\lim_{t \rightarrow \infty} \frac{d\langle\tilde{X}_1(t)\tilde{X}_1(t)\rangle}{dt} = 2\alpha_L |\langle\mathbf{U}^\infty\rangle|, \quad (18)$$

$$\lim_{t \rightarrow \infty} \frac{d\langle\tilde{X}_l(t)\tilde{X}_l(t)\rangle}{dt} = 2\alpha_l |\langle\mathbf{U}^\infty\rangle|, \quad l=2, 3, \quad (19)$$

where $|\langle\mathbf{U}^\infty\rangle|$ is the steady-state value of the average velocity. For given values of $\Gamma_l (l=1, 2, 3)$, the dispersivity tensor, α , can be found numerically by solving Langevin Eqs. (10)–(12) and using relationships Eqs. (18) and (19). Alternatively, for a given α , a model calibration is required to determine Γ_l . A purely mechanical dispersion is impossible to observe or directly measure in laboratory or field experiments because of the ever-present molecular diffusion. But for a porous medium with known pore geometry, the mechanical dispersion coefficient or dispersivity tensor can be found from a solution of the Navier-Stokes equations for pore-scale fluid velocity. Here, we considered the two-dimensional porous medium shown in Fig. 1. A numerical solution of the Navier-Stokes equation for this porous medium was obtained in [21]. We used this solution to calculate the coefficient of mechanical dispersion, and we found $\Gamma_l (l=1, 2)$ for the porous medium through the Langevin model calibration.

III. MULTICOMPONENT REACTIVE TRANSPORT

The Langevin model was used to simulate isothermal steady-state fluid flow and reactive transport of solutes A, B, and C in the homogeneous porous medium. The Langevin simulations were compared with pore and Darcy simulations that were presented in [9]. Examples of the simulations for

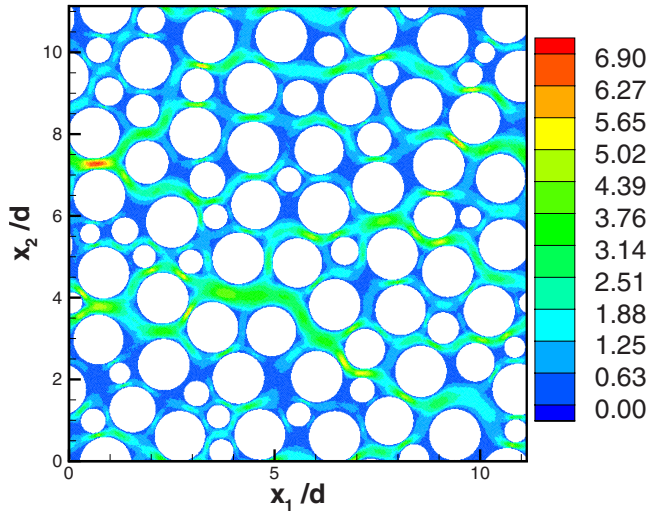


FIG. 1. (Color online) Pore-scale velocity normalized with average pore velocity. Reynolds number $Re=4$. Coordinates x_1 and x_2 are normalized with d , the average grain diameter.

different Peclet numbers are shown in Figs. 2 and 3. Two solutes (A and B) with concentrations A_0 and B_0 were injected into adjacent halves of the porous medium. The solutes underwent mixing along the interface between the two plumes, and the mixing resulted in the irreversible reaction $A+B \xrightarrow{\kappa^*} C$, where κ^* is the reaction rate (with units of volume per time per mole). In the Langevin simulations, the fluid flow and mechanical mixing of the solutes were described by the stochastic flow Eqs. (10) and (12). Diffusive mixing and irreversible reaction between the two solutes A and B are described by the stochastic advection-diffusion-reaction equations:

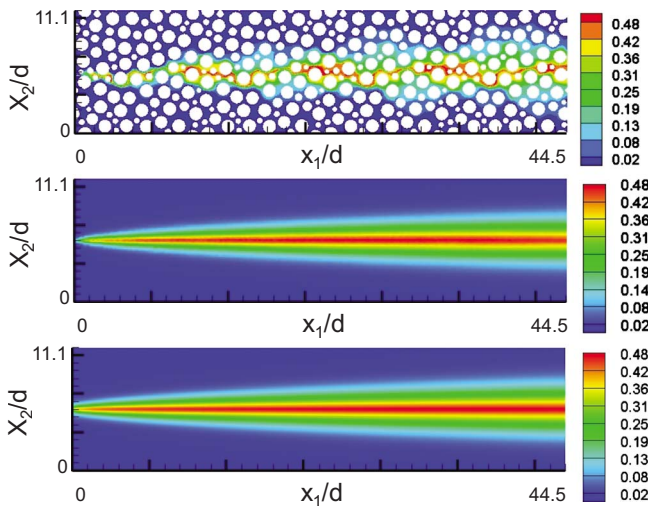


FIG. 2. (Color online) Dimensionless concentration of solute C, a product of the reaction between solutes A and B injected uniformly through the top and bottom halves of the left boundary of the flow domain, for Peclet number $Pe=246$. The top, middle, and bottom panels show results obtained from pore-scale, Langevin, and Darcy simulations, respectively.

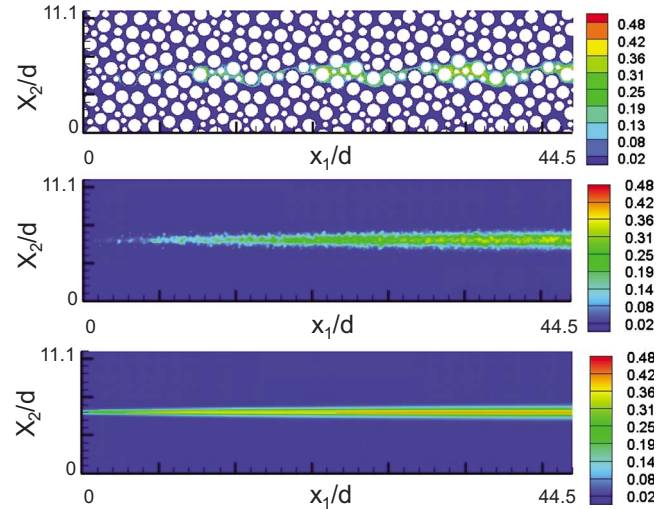


FIG. 3. (Color online) Dimensionless concentration of solute C, a product of the reaction between solutes A and B injected uniformly through the top and bottom halves of the left boundary of the flow domain, for Peclet number $Pe=24610$. The top, middle, and bottom panels show results obtained from microscale, Langevin, and Darcy simulations, respectively.

$$\frac{dA}{dt} = \frac{1}{\rho} \nabla \cdot (\rho D_{eff} \nabla A) - \kappa AB, \quad (20)$$

$$\frac{dB}{dt} = \frac{1}{\rho} \nabla \cdot (\rho D_{eff} \nabla B) - \kappa AB, \quad (21)$$

$$\frac{dC}{dt} = \frac{1}{\rho} \nabla \cdot (\rho D_{eff} \nabla C) + \kappa AB, \quad (22)$$

where A , B are concentrations (mass fractions) of A and B normalized with A_0 and B_0 , C is the concentration of C normalized with A_0+B_0 , and $\kappa = \kappa^* M^*$ (M^* is the referenced molar concentration assumed to be equal to the input molar concentrations of A and B) is the normalized reaction rate with units of one over time. The density of solution ρ was assumed to be independent of concentrations of A, B, and C. This assumption can be easily relaxed [1,17]. The external boundaries of the domain are located at $x_1=0$, $x_1=L_1$, $x_2=0$, and $x_2=L_2$. For simplicity, the parameters Γ_l were determined for the periodic (infinite) porous medium, Sec. V A. Similarly, the dispersion coefficient in the Darcy model was determined for the infinite porous medium [9]. To avoid the effect of boundaries on mechanical dispersion in the Langevin multicomponent reactive transport simulations, velocity and pressure at the boundaries of the domain are assumed to be periodic. These boundary conditions cause average velocity $\langle \mathbf{U} \rangle$ to be in the direction of the body force $\mathbf{g} = (g, 0)^T$. The periodic boundary conditions were also used in the pore-scale multicomponent reactive transport simulations in [9]. At horizontal boundaries located at $x_2=0$ and $x_2=L_2$ normal mass fluxes of A, B, and C are zero. At the vertical boundaries the parallel injection of A and B into different halves of the domain is described by the boundary conditions:

$$A(x_2 < L_2/2) = 1, \quad A(x_2 > L_2/2) = 0, \quad x_1 = 0, \quad (23)$$

$$B(x_2 < L_2/2) = 0, \quad B(x_2 > L_2/2) = 1, \quad x_1 = 0, \quad (24)$$

$$C = 0, \quad x_1 = 0, \quad (25)$$

$$\partial A / \partial x_1 = 0, \quad x_1 = L_1, \quad (26)$$

$$\partial B / \partial x_1 = 0, \quad x_1 = L_1, \quad (27)$$

$$\partial C / \partial x_1 = 0, \quad x_1 = L_1. \quad (28)$$

Initially, the domain is tracer free,

$$A = 0, \quad B = 0, \quad C = 0, \quad t = 0. \quad (29)$$

IV. SPH TRANSPORT EQUATIONS

The Langevin flow and transport Eqs. (10)–(13) were solved with the SPH method. In the SPH Langevin model a fluid is discretized with N_L particles. Positions \mathbf{X}_i^L and velocities \mathbf{U}_i of the particle i ($i=1, \dots, N_L$) are governed by Eqs. (10)–(12) that take the form:

$$\frac{d\mathbf{U}_i}{dt} = -\frac{(\nabla P)_i}{\rho_i} + \mathbf{g} - \gamma_i \mathbf{U}_i + \sqrt{\langle \mathbf{U}_i \rangle} \boldsymbol{\xi}_i, \quad \frac{d\mathbf{X}_i^L}{dt} = \mathbf{U}_i, \quad (30)$$

$$\frac{d\rho_i}{dt} = -\rho_i (\nabla \cdot \mathbf{U})_i, \quad (31)$$

where the subscript i indicates properties associated with the i th particle. The concentration of solute carried by particle i (mass of solute dissolved in particles i divided by the total mass of particle i) does not change as result of advection. Consequently, there is no numerical dispersion in the SPH method, and the solute advection and the mechanical dispersion are treated exactly. The change of the solute concentration carried by particle i due to diffusion-assisted mixing and the reaction is described by the SPH advection-diffusion equations:

$$\frac{dA_i}{dt} = \frac{1}{\rho_i} [\nabla \cdot (\rho D_{eff} \nabla A)]_i - \kappa A_i B_i, \quad (32)$$

$$\frac{dB_i}{dt} = \frac{1}{\rho_i} [\nabla \cdot (\rho D_{eff} \nabla B)]_i - \kappa A_i B_i, \quad (33)$$

$$\frac{dC_i}{dt} = \frac{1}{\rho_i} [\nabla \cdot (\rho D_{eff} \nabla C)]_i + \kappa A_i B_i. \quad (34)$$

SPH discretization of spatial derivatives in Eqs. (30)–(34) is given in the Appendix. In the absence of reactions, SPH discretization conserves mass of each solute exactly. In the presence of reactions the total mass is also conserved.

V. PARAMETRIZATION OF THE STOCHASTIC MODEL

The stochastic transport model was evaluated by comparing its results with pore-scale simulations and predictions of

the Darcy advection-dispersion model. Pore-scale and Darcy simulations of flow and mixing controlled reaction $A+B \rightarrow C$ in the two-dimensional porous medium for several Peclet and Damkohler ($Da = \kappa d^2 / D$) numbers are presented in [9]. Here, we use the solution of the Navier-Stokes equations for fluid flow in the porous medium, shown in Fig. 1, and conservative tracer simulations (numerical solution of the Navier-Stokes equations and tracer simulations were presented in [9]) to calculate the friction coefficient γ and parameters Γ_l ($l=1, 2$) and D_{eff} in the Langevin model.

A. Estimation of γ and Γ_l

The pore-scale fluid flow in the porous medium (Fig. 1) was simulated by solving the continuity and Navier-Stokes Eqs. (1) and (2) subject to the no-flow, no-slip boundary conditions at the grain boundaries and periodic boundary conditions for velocity and pressure at the external boundaries of the periodic domain [9]. The flow was driven by the body (gravitational) force acting in the direction 1. The fluid occupying pore-space was discretized with N_p Lagrangian particles and the solution of the continuity and Navier-Stokes equation was obtained with the SPH method [22]. Figure 1 shows resulting distribution of normalized velocities $\sqrt{v_{1,i}^2 + v_{2,i}^2} / \bar{v}$, where \bar{v} is the average pore velocity in the direction of flow

$$\bar{v} = \frac{1}{N_p} \sum_{i=1}^{N_p} v_{1,i}. \quad (35)$$

The friction coefficient γ was then calculated as

$$\gamma = \frac{g}{\bar{v}}. \quad (36)$$

The coefficients of mechanical dispersion and dispersivities of the porous medium were found from the pore-scale simulation (Fig. 4) using the relationships:

$$\lim_{t \rightarrow \infty} \frac{\partial \sigma_{x_1}^2(t)}{\partial t} = \lim_{t \rightarrow \infty} \frac{\partial}{\partial t} \left[\frac{1}{N_p} \sum_{i=1}^{N_p} \langle \tilde{x}_{1,i}(t) \tilde{x}_{1,i}(t) \rangle \right] = 2D_L^M = 2\alpha_L \bar{v}, \quad (37)$$

and

$$\lim_{t \rightarrow \infty} \frac{\partial \sigma_{x_2}^2(t)}{\partial t} = \lim_{t \rightarrow \infty} \frac{\partial}{\partial t} \left[\frac{1}{N_p} \sum_{i=1}^{N_p} \langle \tilde{x}_{2,i}(t) \tilde{x}_{2,i}(t) \rangle \right] = 2D_T^M = 2\alpha_T \bar{v}, \quad (38)$$

where $\sigma_{x_1}^2$ and $\sigma_{x_2}^2$ are the variances of particle displacements in directions 1 and 2 and

$$\tilde{\mathbf{x}}_i(t) = \mathbf{x}_i(t) - \bar{\mathbf{x}}_i(t). \quad (39)$$

In expression Eq. (39), $\mathbf{x}_i(t)$ is the position of the fluid particle i ($i=1, N_p$) at the time t found from the SPH solution of the Navier-Stokes equations, $\bar{\mathbf{x}}_i(t)$ is the average particle position:

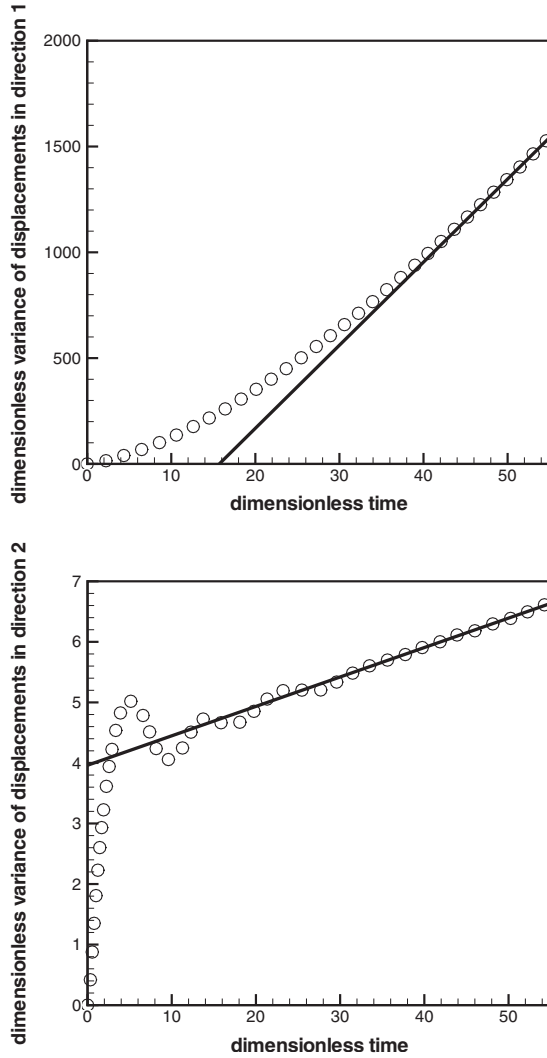


FIG. 4. Open circles represent dimensionless variance of displacements, $\sigma_{x_l}^2/d^2$, versus dimensionless time, $t\bar{v}/d$, obtained from the pore-scale simulation: (a) the variance in the direction 1 (a direction of average flow); and (b) variance in the direction 2 (a direction perpendicular to the direction of average flow). Solid lines are obtained as a best fit to the linear parts of the curves. Components of the dimensionless mechanical dispersion tensor, $2D_L^M/(d\bar{v})$ and $2D_T^M/(d\bar{v})$, are given by the slopes of the solid lines.

$$\bar{\mathbf{x}}_i(t) = \mathbf{x}_i^0 + \frac{1}{N_p} \sum_{j=1}^{N_p} [\mathbf{x}_j(t) - \mathbf{x}_j^0], \quad (40)$$

\mathbf{x}_i^0 is the position of particle i at the time zero, and $\bar{\mathbf{x}}_i(t)$ is the deviation of the position of particle i .

Parameters $\Gamma_1=13.3$ and $\Gamma_2=0.32$, satisfying conditions Eqs. (18) and (19), were found from the Langevin model calibration. Figure 5 shows the variance of the X_1 and X_2 components of the particle position vector, $\langle \tilde{X}_l^2(t) \rangle$ ($l=1,2$), versus time for the stochastic simulation with $\Gamma_1=13.3$ and $\Gamma_2=0.32$ and $\langle \mathbf{U}_i \rangle = \bar{\mathbf{v}} = 0.00535$. The simulation was performed in a two-dimensional rectangular periodic domain filled with $M=8192$ fluid particles. The flow was driven by gravitational body forces acting on the SPH fluid particles.

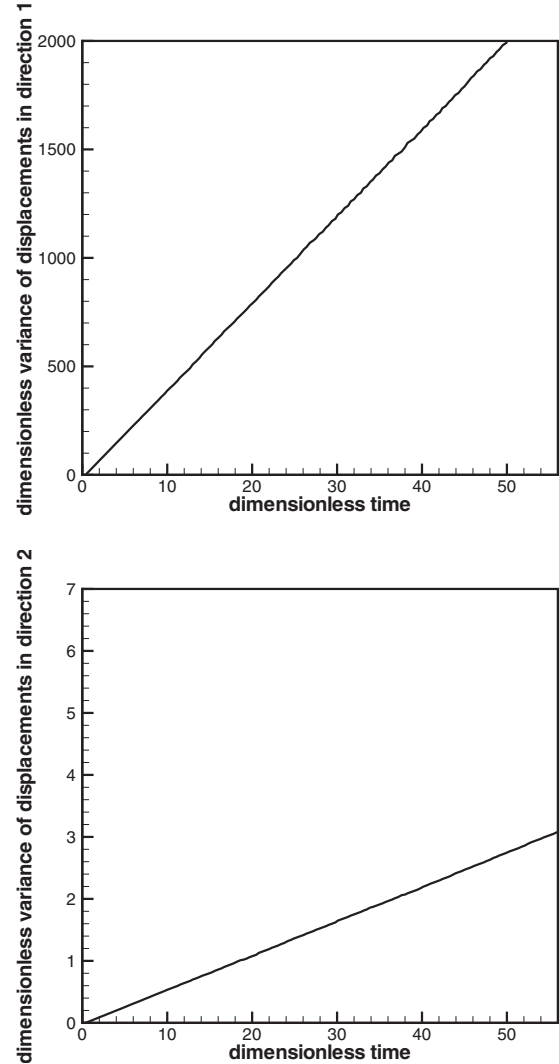


FIG. 5. Dimensionless variance of Lagrangian displacements $\langle \tilde{X}_1^2(t) \rangle/d^2$ in the direction 1 (the left figure) and $\langle \tilde{X}_2^2(t) \rangle/d^2$ in the direction 2 (the right figure) as a function of dimensionless time, $t\bar{v}/d$, obtained from a simulation with $\Gamma_1=13.3$ and $\Gamma_2=0.32$. Components of the dimensionless mechanical dispersion tensor, $2D_L^M/(d\bar{v})$ and $2D_T^M/(d\bar{v})$, are given by the slope of the linear part of the curves.

Because of the periodic boundary conditions, all the fluid particles were statistically equivalent, and the mean velocity and the variance of the Lagrangian displacement of any particle i were the same and could be found from:

$$\langle \mathbf{U} \rangle = \frac{1}{N_L} \sum_{i=1}^{N_L} \mathbf{U}_i, \quad (41)$$

$$\langle \tilde{X}_l^2(t) \rangle = \frac{1}{N_L} \sum_{i=1}^{N_L} (X_{l,i} - \langle X_{l,i} \rangle)^2, \quad l=1,2, \quad (42)$$

and

$$\langle \mathbf{X}_i(t) \rangle = \mathbf{X}_i^0 + \frac{1}{N_L} \sum_{j=1}^{N_L} (\mathbf{X}_j(t) - \mathbf{X}_j^0). \quad (43)$$

TABLE I. Parameters for the Langevin and Darcy transport equations.

Pe	Da	D_m	D_L	D_T	D_{eff}	Langevin error (%)	Darcy error (%)
24.6	1150	6.25×10^{-4}	0.008	0.003	0.0027	3	1
24.6	11500	6.25×10^{-4}	0.008	0.003	0.0027	3	1
246.1	11500	6.25×10^{-5}	0.01	0.0007	6.25×10^{-4}	4	19
24610	115000	6.25×10^{-7}	0.03	0.00003	6.25×10^{-6}	18	52

B. Determination of D_{eff}

Reference [9] presented pore-scale simulations of the advection and diffusion of the conservative tracer in a porous medium made of periodic cell shown in Fig. 1, and determined the dispersion coefficient for this porous medium for different Pe . The longitudinal and transverse components of the dispersion tensor are listed in Table I. Here, we used the values of the dispersion coefficient to determine the transport parameter, D_{eff} , in the Langevin advection-diffusion Eqs. (32)–(34).

The coefficient of effective diffusion D_{eff} in Eqs. (32)–(34) includes the effect of the Taylor-Aris dispersion that is the diffusive solute mixing enhanced by velocity variations inside individual pores. In general, the coefficient of effective dispersion should be a tensor (\mathbf{D}_{eff}). Furthermore, Table I shows that the transverse component of the dispersion tensor increases with increasing D_m and the longitudinal component of the dispersion tensor decreases with increasing D_m . Hence, the form of the dispersion tensor given by Eq. (9) assumes that the longitudinal component of \mathbf{D}_{eff} decreases with increasing D_m and the transverse component of \mathbf{D}_{eff} increases with D_m . The decrease in the longitudinal component of \mathbf{D}_{eff} with increasing D_m is not surprising since the longitudinal component accounts for the Taylor dispersion that is known to decrease with increasing D_m for a given Re [23]. Nevertheless, it is common to replace \mathbf{D}_{eff} with a scalar constant depending only on D_m and porosity and tortuosity of a porous medium [2]. Mixing-induced reactions, considered in this study, are controlled by the transverse component of the dispersion coefficient [24]. To simplify the model without affecting the accuracy of the solution we replaced the \mathbf{D}_{eff} tensor with its transverse component that in the following is denoted by D_{eff} . An extension of the model for the \mathbf{D}_{eff} tensor is relatively straight-forward. Advection of a conservative tracer was simulated to numerically study the dependence of the second moments of the tracer on D_{eff} for Γ_1 and Γ_2 determined in Sec. V A. From this analysis the values of D_{eff} were found to match the transverse dispersion coefficients in the porous medium for $Pe=24.6$, 246, and 24610. These values are given in the Table I and were used in the reactive transport simulations presented below.

VI. NUMERICAL RESULTS AND COMPARISON WITH PORE-SCALE AND DARCY SCALE MODELS

The Langevin model was used for simulations of flow and mixing-induced reactions described by Eqs. (30)–(34) sub-

ject to the initial and boundary conditions Eqs. (23)–(29) in the porous medium shown in Fig. 1 for several Pe and Da . The equations were solved numerically using a smoothed particle hydrodynamics method (see the Appendix). Concentration of the solute C , a product of the irreversible reaction $A+B \rightarrow C$, obtained from the Langevin model for $Pe=246$ and $Da=11500$ is shown in Fig. 2. Figure 3 shows a distribution of C for $Pe=24610$ and $Da=115000$. The Reynolds number was set to $Re=4$. For comparison purposes, Figs. 2 and 3 also show pore scale and Darcy simulations of the same transport phenomena in the same porous medium. Table I gives a summary of all simulations conducted in this study.

The pore-scale simulations show a narrow mixing zone that widens with decreasing Pe . The Darcy model predicted a cone-shaped mixing zone with a Gaussian distribution of C in $x_2(Y)$ direction. On the other hand, the stochastic simulations produced a mixing zone with highly heterogeneous distribution of the solute C . This can be seen very clearly in the simulation with large Pe , Fig. 3. The same phenomenon, but to a smaller degree, is found in the simulation with the smaller Pe (Fig. 6 shows a nonuniform distribution of C in a zoomed-in part of the mixing zone obtained from the Langevin simulation with $Pe=246$).

Reference [10] demonstrated that Darcy-scale equations with constant transport coefficients predict a maximum possible solute dilution and over-predict the real dilution of a tracer in porous media [9], found that over-estimation of dilution increases with decreasing Pe . The over prediction of solute dilution by the Darcy transport model leads to the over-prediction of the mass of C . Figures 7 and 8 show the dimensional mass of C obtained from pore scale, Langevin and Darcy simulations for several Pe and Da :

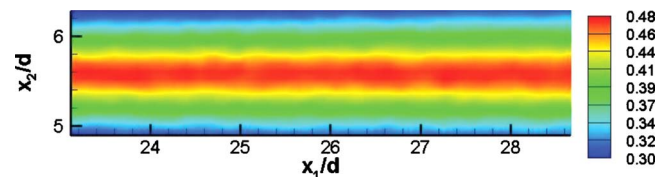


FIG. 6. (Color online) Enlarged view of the mixing zone resulting from the mixing and reaction between two solutes A and B injected uniformly through the top and bottom halves of the left boundary of the flow domain with Peclet number $Pe=246$. The whole computational domain is shown in Fig. 2.

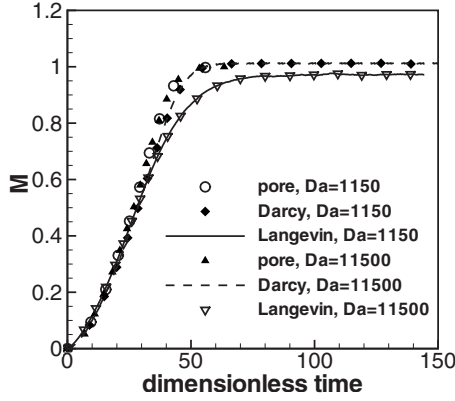


FIG. 7. Dimensionless mass of C versus dimensionless time, $t\bar{v}/d$, obtained from the pore-scale, Langevin and Darcy simulations for $Pe=24$ and different Da . The mass is normalized with respect to the asymptotic value of mass obtained from the pore-scale simulation with corresponding Da .

$$M_I(t) = \frac{\int_{\Omega_I} C_I(\mathbf{x}, t) \rho(\mathbf{x}, t) d\mathbf{x}}{\int_{\Omega_P} C_P(\mathbf{x}, t^*) \rho(\mathbf{x}, t^*) d\mathbf{x}}, \quad (44)$$

where subscript $I=P, L, D$ denotes quantities obtained from pore-scale, Langevin and Darcy model respectively, Ω_I is a computational domain of the corresponding model, and t^* is the time when M_P reaches a steady-state value. The comparison of the three models shows that for small Peclet numbers ($Pe=24$, Fig. 7), both the Langevin and the Darcy models predict mass of C within 3% of the mass of C obtained from the pore-scale model regardless of the magnitude of the Damkohler number. For small Pe , Darcy-scale model appears to be slightly more accurate (1% error) than the Langevin model (3% error). We found that doubling the number of particles reduced the error in the Langevin model by 0.5%. The error is calculated as a relative difference in the total

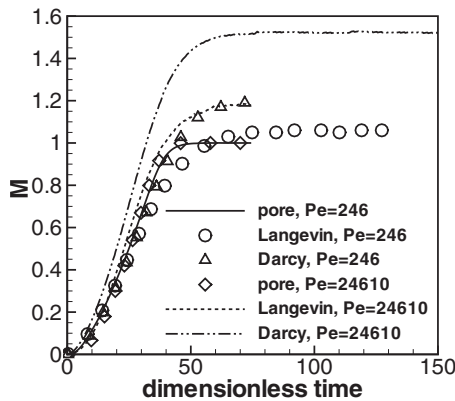


FIG. 8. Dimensionless mass of C versus dimensionless time, $t\langle v \rangle/d$, obtained from the pore-scale, Langevin and Darcy simulations for Peclet numbers $Pe=246$ and $24\,610$. The mass is normalized with respect to the asymptotic value of mass obtained from the pore-scale simulation with corresponding Pe .

mass of C obtained from the pore-scale model and the Langevin or Darcy models. The Damkohler number doesn't have a significant effect on errors in the Langevin and Darcy model predictions. Errors in the Darcy model increase rapidly with increasing Pe , Fig. 8. For $Pe=246$, the relative error in the Darcy model becomes 19%, while the error in the Langevin model stays within 4%. For $Pe=24610$, the relative error in the Darcy model increases to 52%. For $Pe=24610$, the Langevin model remains more accurate than the Darcy model with relative error of 18%. Table I lists the errors in the Langevin and Darcy models for different Peclet and Damkohler numbers. These results show that the separate treatment of mechanical dispersion and molecular and Taylor-type mixing is superior to the effective diffusion (Darcy) model, especially for mixing-controlled reactions with high Peclet numbers.

VII. SUMMARY AND CONCLUSIONS

Recently, we have proposed a phenomenological Langevin model for flow and transport in porous media [1]. In the model, the flow of fluid is governed by a stochastic Langevin equation leading to the mechanical dispersion of the fluid and a solute. Solute mixing due to molecular diffusion and velocity variations within individual pores and pore throats (Taylor dispersion) is governed by the advection-diffusion equation that becomes stochastic due to random advective velocity. The stochastic model separates the effects of diffusive and mechanical mixing on solute transport, while the classical advection-dispersion (Darcy) model assumes a complete mixing (full dilution) on the support of the Darcy model and treats both types of mixing as an effective diffusive process. Here, we extended the Langevin model, originally formulated for isotropic dispersion, to the anisotropic dispersion by using an anisotropic white noise in the Langevin equation.

The Langevin model was used to simulate mixing and reaction between two solutes A and B , injected in parallel into the porous domain for several Peclet and Damkohler numbers. The Langevin transport equations were solved numerically with Smoothed Particle Hydrodynamics. The solution of the Langevin equations was compared with pore-scale and Darcy-scale simulations of the reactive transport in the porous medium for a wide range of Peclet and Damkohler numbers. The parameters in the Langevin and Darcy models were found from pore-scale simulations of a conservative tracer in the porous medium. We found that the Darcy transport model over-estimates the mass of C , a product of irreversible reaction between A and B , with error increasing from 1% for $Pe=24$ to 19% for $Pe=246$ to 52% for $Pe=24610$. The Darcy transport model is accurate for small Pe (when solutes are well mixed on the Darcy support scale). A degree of mixing decreases with increasing Pe and, as a result, the Darcy scale model becomes less accurate and tends to over predict an extend of mixing-controlled reactions. The Langevin model remains accurate within 4% for Pe as large as 246. For $Pe=24610$, the error in the Langevin model increases to 18%, which is significantly smaller than the error in the Darcy model for the same Pe . Peclet numbers

used in the study are within the range of Pe observed in typical sand and gravel aquifers and near injection wells [9,25].

The SPH method is, in general, computationally less efficient than traditional grid-based methods but, due to its similarity to molecular dynamics, a development of highly scalable SPH codes is relatively simple. This should allow performing SPH Langevin simulations of transport problems on scales of practical importance.

ACKNOWLEDGMENTS

This work was supported by the Advanced Scientific Computing Research Program and the Environmental Management Science Program of the U.S. Department of Energy Office of Science. The Pacific Northwest National Laboratory is operated by Battelle for the U.S. Department of Energy under Contract No. DE-AC05-76RL01830.

APPENDIX: SPH LANGEVIN MODEL

1. SPH interpolation scheme

The SPH method is based on the idea that a continuous field $A(\mathbf{X})$ can be approximated as

$$A_I(\mathbf{X}) = \int A(\mathbf{X}') W(|\mathbf{G} \cdot (\mathbf{X} - \mathbf{X}')|) d\mathbf{X}', \quad (\text{A1})$$

where W is the SPH weighting function (a smooth bell-shaped function) with the compact support 1 (in model units of length), $\{W[|\mathbf{G} \cdot (\mathbf{X} - \mathbf{X}')| > 1] = 0\}$, that satisfies the normalization condition:

$$\int W[|\mathbf{G} \cdot (\mathbf{X} - \mathbf{X}')|] d\mathbf{X}' = 1. \quad (\text{A2})$$

\mathbf{G} is the second-rank tensor. The form of \mathbf{G} depends on the dimensionality of the space. In 2D \mathbf{G} takes the form:

$$\mathbf{G} = \begin{pmatrix} h_1^{-1} \cos^2 \psi + h_2^{-1} \sin^2 \psi & (h_1^{-1} - h_2^{-1}) \cos \psi \sin \psi \\ (h_1^{-1} - h_2^{-1}) \cos \psi \sin \psi & h_1^{-1} \sin^2 \psi + h_2^{-1} \cos^2 \psi \end{pmatrix}, \quad (\text{A3})$$

where h_1 and h_2 are the semimajor and semiminor axes of the ellipse and ψ is the angle between coordinate 1 and semimajor axis. If semimajor axis of the ellipse coincides with the direction of the coordinate 1, then \mathbf{G} reduces to:

$$\mathbf{G} = \begin{pmatrix} h_1^{-1} & 0 \\ 0 & h_2^{-1} \end{pmatrix}. \quad (\text{A4})$$

In the $h_1 \rightarrow 0$ limit, W is required to reduce to the Dirac delta function. In this limit the SPH interpolation scheme becomes exact, i.e., $A_I \equiv A$. To simplify notation, in the following we will drop the subscript I .

In a numerical implementation of the SPH method, fluids occupying a computational domain are represented by a set of N particles with positions $\mathbf{X}_i (i=1, N)$ and the integral in Eq. (A1) is discretized as

$$A_i = \sum_j A_j / n_j W(|\mathbf{G} \cdot (\mathbf{X}_i - \mathbf{X}_j)|), \quad (\text{A5})$$

where $A_i = A(\mathbf{X}_i)$; $n_i = \rho_i / m_i$ is the particle number density; and m_i is the mass of particle i . The SPH approximation for continuous fields allows the mass and momentum conservation equations to be written in the form of a system of ordinary differential equations (ODEs) [19].

2. SPH equations

Using the SPH interpolation scheme Eq. (A5), the Langevin Eq. (10) can be discretized as [20]:

$$\frac{d\mathbf{U}_i}{dt} = \mathbf{F}_i^A + \mathbf{F}_i^B, \quad (\text{A6})$$

where

$$\mathbf{F}_i^A = -\frac{1}{m_i} \sum_j \left(\frac{P_j}{n_j^2} + \frac{P_i}{n_i^2} \right) \nabla_i W(|\mathbf{G} \cdot \mathbf{X}_{ij}|) + \mathbf{g} - \gamma_i \mathbf{U}_i, \quad (\text{A7})$$

$$\mathbf{F}_i^B = \sqrt{|\langle \mathbf{U}_i \rangle|} \boldsymbol{\xi}_i, \quad (\text{A8})$$

where $\mathbf{X}_{ij} = \mathbf{X}_i - \mathbf{X}_j$; \mathbf{U}_i is the velocity of particle i ; $|\langle \mathbf{U}_i \rangle| = \sqrt{\sum_{k=1}^{D_s} (\int_V U_k d\mathbf{x} / V)^2} = \sqrt{\sum_{k=1}^{D_s} (\sum_{i=1}^{N_L} U_{k,i} / n_i / V)^2}$; $V = \sum_{i=1}^{N_L} 1 / n_i$ is the volume of the computational domain where the Langevin equations is defined; D_s is the number of spatial dimensions; m_i is the mass of particle i . The evolution of particle density, n_i , can be found directly from Eq. (A5) with $A = n$:

$$n_i = \sum_j W(|\mathbf{G} \cdot \mathbf{X}_{ij}|), \quad (\text{A9})$$

and Eq. (A9) replaces the continuity Eq. (12) [19]. The first term on the right hand side of Eq. (A7) is obtained through SPH discretization of $(\nabla P)_i / \rho_i$ in Eq. (10) [19]. The system of equations is closed by the equation of state,

$$P_i = P_{eq} n_i / n_{eq}, \quad (\text{A10})$$

where n_{eq} is the average number of particles per unit volume and P_{eq} is the pressure of the particles in the equilibrium state (the state in which the total force acting on each particle is zero in the absence of body and random forces).

The SPH formalism can also reduce the diffusion Eqs. (20)–(22) to the system of ODEs [22]:

$$\begin{aligned} \frac{d(A, B)_i}{dt} &= \frac{D_{eff}}{m_i} \sum_j \frac{(m_i n_i + m_j n_j) (A, B)_{ij}}{n_i n_j \mathbf{X}_{ij}^2} \mathbf{X}_{ij} \cdot \nabla_i W(|\mathbf{G} \cdot \mathbf{X}_{ij}|) \\ &\quad - \kappa A_i B_i, \end{aligned} \quad (\text{A11})$$

$$\frac{dC_i}{dt} = \frac{D_{eff}}{m_i} \sum_j \frac{(m_i n_i + m_j n_j) C_{ij}}{n_i n_j \mathbf{X}_{ij}^2} \mathbf{X}_{ij} \cdot \nabla_i W(|\mathbf{G} \cdot \mathbf{X}_{ij}|) + \kappa A_i B_i, \quad (\text{A12})$$

where $a_{i,j} = a_i - a_j (a = A, B, C)$ and A_i , B_i , and C_i are the concentrations of solutes A, B and C carried by particle i . For simplicity, all SPH particles have mass m_0 that is indepen-

dent of the solute concentration. The assumption of a highly dilute solution can be easily relaxed [1].

In general, different forms of $\mathbf{G}=\mathbf{G}(h_1, h_2)$ can be used in different equations. It is common in SPH to use G with $h_1=h_2$ (isotropic W kernel) in which case the SPH interpolation scheme Eq. (A5) approximates a function at \mathbf{X} with a weighted spatial average inside a circle (sphere in three dimensions) centered at \mathbf{X} . In a general case of $h_1 \neq h_2$ (anisotropic W kernel), a function is approximated with a weighted average inside an ellipse (ellipsoid in three dimensions). The use of isotropic kernel W is appropriate when “noise” in a partial differential equation is isotropic or completely absent. Isotropic kernel $W [h_1=h_2=1$ (in model units of length)] was used in the SPH diffusion Eqs. (A11) and (A12). In the SPH Langevin equation the random noise is anisotropic ($\Gamma_1=13.3$ and $\Gamma_2=0.32$), and this required the use of the anisotropic kernel W . In the simulations, $h_1=10$ and $h_2=1$ (in model length units) were used in the SPH Eqs. (A6)–(A9).

The implementation of the SPH model is straightforward and consists of the following 5 steps:

Step 1. The fluid is discretized by placing randomly or uniformly $N_L=n_{eq}V$ particles throughout the computational domain with volume V . The initial velocity and concentration are assigned to each particle.

Step 2. The number densities of all particles, n_i , are calculated from Eq. (A9) and the pressures, P_i , are found from the equation of state Eq. (A10).

Step 3. $N_L N_S$ random numbers (N_S is the number of spatial dimensions) from the standard normal distribution, $\zeta_{l,i}$ ($l=1, \dots, N_S$, $i=1, \dots, N_L$) are generated and the random forces in Eq. (A8) are calculated according to $\xi_{l,i}=\Gamma_l \zeta_{l,i}$. The total forces acting on each fluid particle and the rate of change of solutes concentrations dissolved in each particles are calculated from Eqs. (A6)–(A8), (A11), and (A12).

Step 4. The new positions, velocities of the fluid particles and solutes concentration are found by time integration of Eqs. (A6), (A11), and (A12) using the explicit “velocity Verlet” algorithm [26] which takes the form:

$$\mathbf{X}_i^{t+\Delta t} = \mathbf{X}_i^t + \Delta t \mathbf{U}_i^t, \quad (\text{A13})$$

$$I_i^{t+\Delta t} = I_i^t + \frac{\Delta t}{2} \left(\left. \frac{dI}{d\tau} \right|_{\tau=t+\Delta t} + \left. \frac{dI}{d\tau} \right|_{\tau=t} \right), \quad I=A, B, C, \quad (\text{A14})$$

and

$$\mathbf{U}_i^{t+\Delta t} = \mathbf{U}_i^t + \frac{\Delta t}{2} (\mathbf{F}_i^{A,t+\Delta t} + \mathbf{F}_i^{A,t}) + \frac{\sqrt{\Delta t}}{2} (\mathbf{F}_i^{B,t+\Delta t} + \mathbf{F}_i^{B,t}). \quad (\text{A15})$$

The time step in Eqs. (A13)–(A15) is determined from the CFL stability condition [20]. After the positions of the fluid particles are updated according to Eq. (A13), Steps 2–4 are repeated.

3. Boundary conditions

In the flow simulations, periodic boundary conditions were used. Fluid particles, exiting the computational domain, were returned to the flow domain through the opposite boundary with the same velocities. The periodic boundary conditions were used to avoid the effect of the boundaries on the mechanical dispersion.

The boundary conditions, Eqs. (23)–(28) for the advection-diffusion-reaction equations were imposed as the following: the concentrations $A=A_0$, $B=0$, and $C=0$ were assigned to the particles entering at $x_1=0$ in the top half of the domain and $A=0$, $B=B_0$, and $C=0$ in the bottom half of domain. Symmetry with respect to $x_2=L_2/2$ was used to impose zero-mass flux condition at the $x_2=0$ and $x_2=L_2$ boundaries: the particle i with concentrations A_i , B_i , and C_i exiting boundary at $x_2=0$ were returned to the domain through the boundary at $x_2=L_2$ with concentrations $A_i^*=B_i$, $B_i^*=A_i$, and $C_i^*=C_i$. Similarly, the particle i with concentrations A_i , B_i , and C_i exiting boundary at $x_2=L_2$ were returned to the domain through the boundary at $x_2=0$ with concentrations $A_i^*=B_i$, $B_i^*=A_i$, and $C_i^*=C_i$.

-
- [1] A. M. Tartakovsky, D. M. Tartakovsky, and P. Meakin, *Phys. Rev. Lett.* **101**, 044502 (2008).
- [2] J. Bear, *Dynamics of Fluids in Porous Media* (Dover, New York, 1988).
- [3] J. Li and D. Helm, *Water Resour. Res.* **34**, 1675 (1998).
- [4] D. Koch and J. Brady, *J. Fluid Mech.* **154**, 399 (1985).
- [5] J. Carvalho and J. Delgado, *Chem. Eng. Sci.* **54**, 1121 (1999).
- [6] A. Olsson and P. Grathwohl, *J. Contam. Hydrol.* **92**, 149 (2007).
- [7] C. Knutson, A. Valocchi, and C. Werth, *Adv. Water Resour.* **30**, 1421 (2007).
- [8] O. Cirpka, E. Frind, and R. Helmig, *J. Contam. Hydrol.* **40**, 159 (1999).
- [9] A. M. Tartakovsky, G. D. Tartakovsky, and T. D. Scheibe, *Adv. Water Resour.* **32**, 1674 (2009).
- [10] P. Kitanidis, *Water Resour. Res.* **30**, 2011 (1994).
- [11] N. Van Kampen, *Stochastic Processes in Physics and Chemistry* (Elsevier, New York, 2001).
- [12] R. Maier, D. Kroll, R. Bernard, S. Howington, J. Peters, and H. Davis, *Phys. Fluids* **12**, 2065 (2000).
- [13] J. H. Cushman, D. O’Malley, and M. Park, *Phys. Rev. E* **79**, 032101 (2009).
- [14] E. LaBolle, G. Fogg, and A. Tompson, *Water Resour. Res.* **32**, 583 (1996).
- [15] T. Le Borgne, M. Dentz, and J. Carrera, *Phys. Rev. Lett.* **101**, 090601 (2008).
- [16] D. Fernández-García, X. Sanchez-Vila, and T. Illangasekare, *J. Contam. Hydrol.* **57**, 129 (2002).
- [17] A. Tartakovsky and P. Meakin, *J. Comput. Phys.* **207**, 610 (2005).
- [18] D. Benson and M. Meerschaert, *Water Resour. Res.* **44**, W12201 (2008).

- [19] J. Monaghan, *Rep. Prog. Phys.* **68**, 1703 (2005).
- [20] W. Welton and S. Pope, *J. Comput. Phys.* **134**, 150 (1997).
- [21] A. M. Tartakovsky and S. P. Neuman, *Geophys. Res. Lett.* **35**, L21401 (2008).
- [22] A. Tartakovsky, P. Meakin, T. Scheibe, and B. Wood, *Water Resour. Res.* **43**, W05437 (2007).
- [23] R. Aris, *Proc. R. Soc. London, Ser. A* **235**, 67 (1956).
- [24] R. Acharya, A. Valocchi, C. Werth, and T. Willingham, *Water Resour. Res.* **43**, W10435 (2007).
- [25] T. Harter, *Basic Concepts of Groundwater Hydrology* (University of California, Berkeley, 2003).
- [26] M. P. Allen and D. J. Tildesley, *Computer Simulation of Liquids* (Oxford University Press, Oxford, 2001), p. 81.